Backtracking depth-resolved microstructures for crystal plasticity identification – Part 1: Backtracking microstructures

Qiwei Shi, Félix Latourte, François Hild, Stéphane Roux

Backtracking depth-resolved microstructures for crystal plasticity identification – Part 1: Backtracking microstructures

Qiwei Shi[1,2,*], Félix Latourte[2], François Hild[1], Stéphane Roux[1]
1: LMT, ENS Paris-Saclay / CNRS / Université Paris-Saclay,
61 avenue du Président Wilson, F-94235 Cachan (FRANCE)
2: EDF R&D, Site des Renardières,
avenue des Renardières, Ecuelles, F-77818 Moret-sur-Loing (FRANCE)

Email: qshi@lmt.ens-cachan.fr

Abstract

In-situ mechanical tests performed on polycrystalline materials in a scanning electron microscope suffer from the lack of information on depth-resolved 3D microstructures. The latter ones can be accessed with focused ion beam technology only postmortem, because it is destructive. The present study considers the challenge of backtracking this deformed microstructure to the reference state. This theoretical question is tackled on a numerical (synthetic) test case. A 2D microstructure with one dimension along the depth is considered, and deformed using a crystal plasticity law. The proposed numerical strategy is shown to retrieve accurately the reference state.

Keyword: Crystal plasticity, finite element model updating, boundary conditions

1   Introduction

Many enrichments of multiscale plasticity constitutive models have been proposed in the past decades, which are motivated by better predictions of the macroscopic behavior. In this context, validations of crystal plasticity models exploiting kinematic fields have been conducted, and more specifically the displacement and strain fields obtained from images acquired with a Scanning Electron Microscope (SEM) [1, 2, 3]. However, only surface measurements are accessible. For the purpose of validating the identification procedure and its upscaling to macroscopic laws, samples with columnar and coarse grains have been prepared so that mere extrusion of the surface microstructure is a valid description [2]. Such an approach has the merit of addressing the methodology with a good control of the microstructure. Yet, it is limited to materials that are not representative of most key applications. If a similar procedure, *e.g.,* extrusion of the observation face microstructure, is applied to materials with unknown grain geometry in the depth direction, numerical modeling is expected to lead to poor agreement with *in-situ* observations, as documented from numerous numerical simulations (see *e.g.,* [4]). Another option is to generate in-depth microstructure synthetically based on surface grain structures, which introduces randomness into models. Nonetheless, numerous works have adopted extruded model from surface [3] or synthetic in-depth microstructure [5] in 3D simulations, due to the lack of real 3D microstructures. It is believed that any progress achieving a better determination of the microstructure will lead to much more constrained, and hence reliable, identification.

The large avenue to access 3D microstructures, which is compatible with a broad class of materials, is to consider 3D-FIB SEM tomography also known as 3D-EBSD [6, 7]. This technique consists of EBSD characterization of surfaces obtained after successive FIB milling, which progressively reveals the material in depth. Such technique allows for very fine spatial resolutions down to 50 nm, and very accurate crystallographic orientations (about $0.5°$). Microstructure models have for instance benefited from this technique [8]. The limitation of 3D-EBSD is its *destructive* character, which may lead to the erroneous conclusion that it is not compatible with an *in-situ* mechanical test. In fact, 3D-EBSD could be performed but only at the end of the mechanical test, and hence after potentially large deformations, whereas a standard mechanical model requires the knowledge of the undeformed state.

The present study aims at addressing the feasibility of backtracking the 3D depth-resolved microstructure of the final state to the initial one, in order to increase the reliability of interpretations of surface characterizations of mechanical tests performed *in-situ* (*i.e.,* in an SEM). The surface deformation of sample surfaces can be measured thanks to full-field measurement techniques such as Digital Image Correlation [9, 10, 1]. More recently, it was shown that the crystal rotation fields can also be measured on surfaces by registering EBSD images via so-called quaternion correlation [11]. The active slip systems can also be revealed since they induce surface roughness detected in SEM pictures [12, 13]. High angular resolution EBSD provides insight into the surfaces residual deformation at each step [14]. All this detailed information is specific from the observed surface, and as previously mentioned, without a reliable 3D microstructure, it remains uncomplete for mechanical models.

To the best of the authors' knowledge, such a problem definition has never been addressed in the past and in particular the limitations due to its ill-posed character (although reduced as compared to bare surface measurements) are difficult to assess. Hence, a 2D (*i.e.,* one surface and one depth directions) synthetic problem is considered in the following, because of the high numerical cost of the direct and inverse modeling. It is believed that the issue of depth is well captured by such a simplified approach, though surface measurements are much poorer in the present 2D problem than in real 3D cases.

The paper is organized as follows. Section 2 details the proposed procedure to determine the reference configuration. Section 3 is dedicated to a virtual experiment carried out to validate the results. The most important benefit of retrieving the microstructure underneath the surface is for the identification of a constitutive law. This question is addressed in a companion paper [15].

2 Proposed procedure

2.1 Definition of the problem

Modeling *in-situ* mechanical tests at the microstructure scale, requires two types of unknowns, namely, the reference configuration Ω_{ref} of the microstructure and the constitutive equation parameters $\{p\}$ (assuming the constitutive law itself is either known or chosen). The configuration Ω_{ref} consists here only in the crystal orientation Ξ — parameterized with *e.g.,* Euler angles or quaternions — at each material point X. Additional internal parameters that could be included in this configuration are here ignored.

From 3D-EBSD analyses, it is assumed that what is known is the deformed configuration Ω_{def}^{exp}, namely the field of crystal orientation ξ at each material point x of the deformed geometry. From surface SEM observations and digital image correlation, the Lagrangian displacement field $u^{exp}(X, t)$ is known for X at the observed surface only, and in the course of time (or loading) t. Additional measurements may be available such as the remote load $F^{exp}(t)$.

In continuum mechanics, the displacement field is the only relevant kinematic field, and hence modeling consists in computing the transformation of the reference material points, X, into new position x at any stage t of loading

$$x = \Phi(X, t) \equiv X + u(X, t) \tag{1}$$

where $u(X)$ is the Lagrangian displacement field. For crystal plasticity, an enriched description is required, as each material point is endowed with its crystal orientation, and its evolution in the course of plastic flow has to be accounted for. Hence, the generalized or enriched kinematic transformation has to be considered, where both current position *and* orientation (x, ξ) have to be related to their initial state (X, Ξ). Thus the configuration $\Omega_{ref} = \Xi(X)$ is transformed into a deformed one $\Omega_{def} = \xi(x)$ as described by a generalized transformation still denoted by Φ

$$(x, \xi) = \Phi(X, \Xi, t) \tag{2}$$

where the dependence with respect to the reference orientation has been made explicit, although a given finite element simulation only computes Φ for a given configuration since the constitutive law itself depends on the crystal orientation, and hence only the restriction $\widehat{\Phi}(X, t) = \Phi(X, \Xi(X), t)$ is directly accessible.

It is to be emphasized that model error, *i.e.,* the fact that the actual plasticity behavior would not be described by the chosen constitutive law, is not considered herein. It is a very important and often limiting point, however addressing such a problem is beyond the ambition of the present study. In the following, it will be assumed that the algebraic form of the law and the relevant internal parameters are correct.

2.2 Microstructure estimate

The present procedure is designed to estimate the reference configuration from the deformed one assuming that the constitutive law is close to the actual one. It is sketched in Figure 1, which accounts for the left part of Figure 1 in the second part of the study [15]).
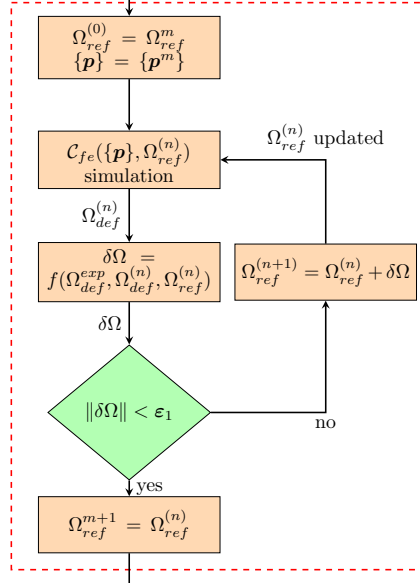

Figure 1: Flowchart describing the determination of the reference configuration

In this procedure, the inputs are:
- the material parameters $\{\boldsymbol{p}^m\}$ that are assumed to be known and are not updated;
- an initial estimate of the reference configuration $\Omega_{ref}^{(0)}$ that will be updated iteratively (index n);
- boundary conditions prescribed on the reference configuration during FE analyses;
- experimental kinematic field $\{\boldsymbol{u}^{exp}\}_t$, experimental loading force $\{\boldsymbol{F}^{exp}\}_t$.

The output is an updated estimate of the reference configuration, which approaches at best the exact yet unknown reference configuration Ω_{ref}^{exp}. In order to proceed with the FE computation of the deformed configuration (*i.e.,* the so-called direct problem), the boundary conditions are needed. The observed free surface is very well documented since the surface displacement field is known (*i.e.,* measured), and it is traction-free. Hence both Dirichlet and Neumann conditions could be used. This redundancy will be used in the following. However, in depth, the information is lacking and has to be inferred. Various prescriptions can be envisioned to guess a depth extrapolated displacement field, which is compatible with surface displacements. None of them will be exact, but it may be expected that the errors due to the extrapolation will mostly affect the boundary of the studied domain, and that the central part of the observed surface will only be marginally dependent on the boundary condition prescription. This question will be addressed in Section 3.

With the reference configuration, the constitutive law and boundary conditions (as defined through a given prescription), an appropriate finite element computation provides the (generalized) transformation Φ

$$(\boldsymbol{x}(\boldsymbol{X}), \boldsymbol{\xi}(\boldsymbol{X})) = \Phi(\boldsymbol{X}, \boldsymbol{\Xi}, t) \tag{3}$$

The difficulty is to solve the inverse problem. The proposed strategy is a simple correction step based on an approximation of the tangent transformation. Let us consider a small modification of the reference configuration, $\mathrm{d}\boldsymbol{\Xi}(\boldsymbol{X})$, and study its effect in the deformed configuration

$$(\boldsymbol{x}(\boldsymbol{X}) + \boldsymbol{\delta x}(\boldsymbol{X}), \boldsymbol{\xi}(\boldsymbol{X}) + \boldsymbol{\delta \xi}(\boldsymbol{X})) = \Phi(\boldsymbol{X}, \boldsymbol{\Xi} + \boldsymbol{\delta \Xi}(\boldsymbol{X}), t) \tag{4}$$

In the most general terms, it can be written as involving nonlocal but linear operators

$$\boldsymbol{\delta x}(\boldsymbol{X}) = \int \boldsymbol{G}_1(\boldsymbol{X}, \boldsymbol{X}')\boldsymbol{\delta \Xi}(\boldsymbol{X}')\, \mathrm{d}\boldsymbol{X}'$$

$$\boldsymbol{\delta \xi}(\boldsymbol{X}) = \int \boldsymbol{G}_2(\boldsymbol{X}, \boldsymbol{X}')\boldsymbol{\delta \Xi}(\boldsymbol{X}')\, \mathrm{d}\boldsymbol{X}' \tag{5}$$

3

Let us note that this explicit computation is prohibitive as it requires multiple finite element computations for any perturbation $\boldsymbol{\delta\Xi}(\boldsymbol{X})$. Therefore it is proposed to use a very simple approximation of these transformations $\boldsymbol{G}_1$ and $\boldsymbol{G}_2$, trivially inverted in order to update the reference configuration based on observed differences in the deformed configurations.

An additional specificity of the crystalline microstructure that is addressed herein is that roughly, each crystal i is considered to have a unique orientation, $\boldsymbol{\Xi}_i$ and hence only the grain boundaries matter. Moreover, crystals are considered to be polyhedral in 3D (resp. polygonal in 2D) and hence can be defined by a set of triplets (resp. doublets) of points, which define local facets from a connectivity table. The latter defines the granular *topology* that is believed not to be affected by the plastic deformation and thus that can be read from the deformed state. Therefore only the coordinates of these vertices A_j, $\boldsymbol{X}(A_j)$, (akin to finite element nodes) contribute to the definition of the deformed granular system. These vertices are also physical points lying at grain boundaries. The set of discrete orientations $\boldsymbol{\Xi}_i$, one per grain, and of vertices $\boldsymbol{X}(A_j)$ forming the grain boundaries, is a natural parameterization of the granular configuration. Within iteration n of the procedure, the deformed state $\boldsymbol{\xi}_i^{(n)}$ and $\boldsymbol{x}(A_j)^{(n)}$ is computed.

Because the sought microstructure is piecewise constant, the considered perturbations are mainly of two types. The first corresponds to a slight variation of the orientation uniformly within each crystal at fixed shape. The second type is a slight modification of the boundary between grains at fixed orientation. This is a convenient representation of the *residual* difference between the computed and observed configuration. Within each crystal, i, the mean difference of orientation $\Delta\boldsymbol{\xi}_i^{(n)} = \boldsymbol{\xi}_i^{exp} - \boldsymbol{\xi}_i^{(n)}$ is of the first type, whereas the differences of position $\Delta\boldsymbol{x}^{(n)}(A_j) = \boldsymbol{x}^{exp}(A_j) - \boldsymbol{x}^{(n)}(A_j)$ for each face vertex, j, easily identified from topological features, make up the second type.

For the first case, the approximations $\widetilde{\boldsymbol{G}}_1(j, j') = \boldsymbol{0}$ and $\widetilde{\boldsymbol{G}}_2(i, i') = \delta_{ii'}\boldsymbol{I}$ are chosen. Hence, the observed crystal misorientation between computed and observed configurations in the deformed state is simply corrected by the same amount locally, *i.e.*, per crystal without altering its shape. For the second case, the mispositioning of a vertex is transported back to the reference configuration again locally, *i.e.*, without affecting other vertices, and identically, *i.e.*, with no alteration of the magnitude and orientation of the mispositioning ΔA_j. Likewise, the crystal orientations are unaltered. In other words, the approximations $\widetilde{\boldsymbol{G}}_1(j, j') = \delta_{jj'}\boldsymbol{I}$ and $\widetilde{\boldsymbol{G}}_2(i, i') = \boldsymbol{0}$ are chosen. Therefore, the differences noted in the deformed state are directly accounted for in the reference configuration

$$
\begin{array}{rcl}
\boldsymbol{X}^{(n+1)}(A_j) & = & \boldsymbol{X}^{(n)}(A_j) + \boldsymbol{x}^{exp}(A_j) - \boldsymbol{x}^{(n)}(A_j) \\
\boldsymbol{\Xi}_i^{(n+1)} & = & \boldsymbol{\Xi}_i^{(n)} + \boldsymbol{\xi}_i^{exp} - \boldsymbol{\xi}_i^{(n)}
\end{array}
\tag{6}
$$

This step defines one iteration of the microstructure correction, which is repeated until a stationary condition is observed, namely, until incremental changes in $\boldsymbol{X}(A_j)$ or $\boldsymbol{\Xi}_i$ are considered as small enough, *i.e.*, less than a given parameter ε_1. It should be emphasized that to solve the inverse problem, iterations of the direct method have been adopted to evaluate the sought answer. The inversion of the constitutive law and related possible instabilities have been avoided at the price of multiple direct calculations.

3 Proof of concept

3.1 Virtual experiment

In the following a 2D synthetic test case is considered in order to study the feasibility of the proposed procedure by comparing the result Ω_{ref} with known values. In 2D, the top edge of the considered model corresponds to the observation surface whereas the vertical direction is along the depth. The displacement field is computed from a Finite Element simulation with Code_Aster [16]. A two-dimensional microstructure shown in Figure 2 with isotropic texture is modeled. It corresponds to an experimental orientation map of a reactor pressure vessel steel sample [17]. Two sets of isotropic crystallographic orientations are generated randomly, each being uniform inside each crystal, as shown in Figures 2(a) and 2(b). This domain represents a large scale medium at the boundary of which simple conditions are applied. It is meshed as shown in Figure 2(c) conforming to the grain shapes. The finite element computation is performed under a plane strain assumption. The entire domain is subjected to a monotonic uniaxial tensile strain up to 6 % with the following boundary conditions. The left and right edges both have uniform displacements in the x (horizontal) direction. All data extracted from the simulations are designated as "experimental" in the following.
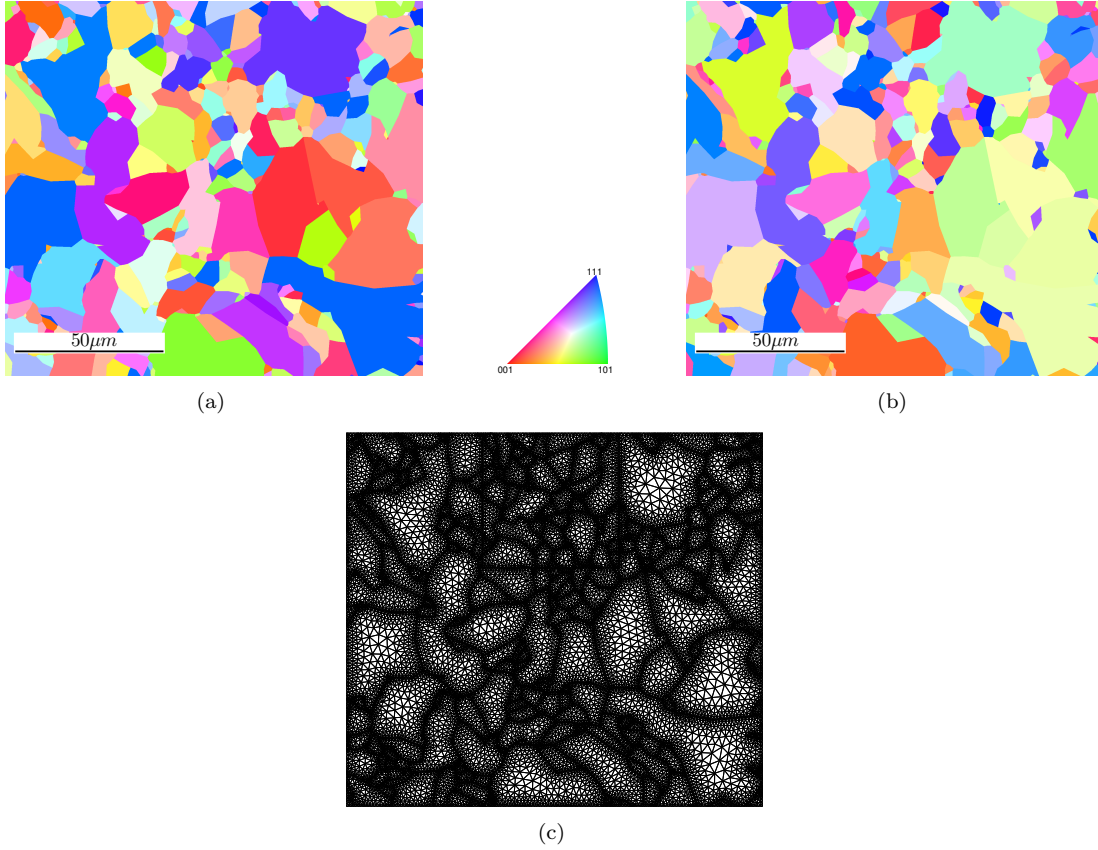
Figure 2: (a) Inverse pole figure of the 2D polycrystalline model, orientation set 1 (a) and set 2 (b). (c) FE mesh of the virtual experiment. The square region at the top, of size $50\mu m \times 50\mu m$, is the region of interest (ROI) before deformation, *i.e.,* Ω_{ref}^{exp}

A constitutive law based on dislocation dynamics for body centered cubic crystals (DD_CC [18]) has been chosen in the FE simulations. A finite strain framework is used to implement the constitutive equations in order to properly account for crystal rotation during the applied load.

In order to be representative of future experiments, a smaller square Region Of Interest (ROI) is defined. Its size is one third of the initial domain in each direction. It is centered in the horizontal direction, and attached to the free surface along the vertical direction. This ROI mimics the region that would be analyzed using 3D-EBSD. The surrounding part is introduced as a buffer zone that mediates a uniform displacement applied on the outer boundary to a more "natural" one at the edges of the ROI.

The grain boundaries of the global model using orientation set 1 before (black) and after (blue) straining the sample are shown in Figure 3(a), and the grain boundaries inside the ROI are shown in Figure 3(b). The blue lines in Figure 3(b) indicate the grain boundaries of the deformed configuration Ω_{def}^{exp}, which would be available in real-life experiments by postmortem 3D-EBSD. Note that Ω_{def}^{exp} will be the starting point of all the following calculations.
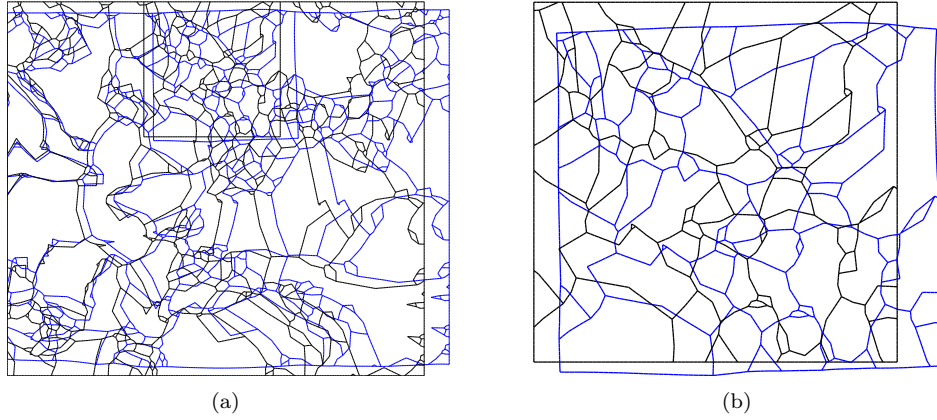
Figure 3: Reference (in black) and deformed (in blue) configurations of the the whole model (a) and the region of interest (b) of the virtual experiment

3.2   Choice of boundary conditions

Boundary conditions (BCs) are essential in crystal plasticity calculations and strongly affect the mechanical response of grains in the vicinity of the boundary. Figure 4(a) provides an illustration of nodal displacements obtained by a first direct calculation during which the domain Ω is surrounded by a polycristalline material providing realistic grain-to-grain interaction effects at the boundary $\partial\Omega$. During the reconstruction procedure, the estimated microstructure is loaded with the BCs depicted in Figure 4(b). Only the two upper corners are loaded with the exact two components of the displacement that can be measured experimentally, and drawn in blue color in Figure 4(a). As the subsurface displacement is unknown (red arrows in Figure 4(a)), assumptions have to be made to circumvent the lack of information while obtaining a mechanical response as close as possible from the reference solution, especially at the specimen surface where the model validation is conducted. Artifacts in boundary conditions will mostly affect the response of grains surrounding the boundary.
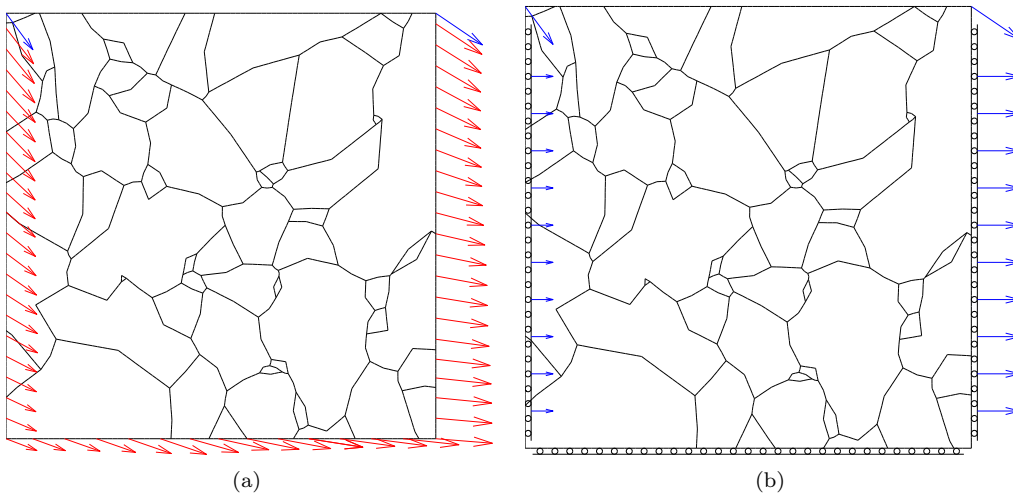

Figure 4: Comparison of boundary conditions. (a) exact BC applied on the model, extracted from the synthetic experiment calculations; (b) adopted BC for all of the FE analyses.

A preliminary assumption consists in applying a uniform normal displacements along the three subsurface edges as shown in Figure 4(b). Tangential displacements are not prescribed. For the two side edges, the normal displacement is equal to that of the relative upper corner. For the bottom edge, the normal displacement is uniform but let free providing an absence of global reaction in the vertical direction. The upper edge is naturally under a traction free condition. After assessing several other simple assumptions in a preliminary work, the BCs shown in Figure 4(b) have been kept for all the remaining analyses. Since errors are known to result from the discrepancy between exact BCs and assumed BCs, quantifications will be provided hereafter.

3.3 Initialization of the configuration Ω_{ref}^0

To initialize the iterative process, one may choose Ω_{def}^{exp} as Ω_{ref}^0. However, a very simple constitutive equation, namely, macroscopic pseudo-elasticity, is adopted to provide the first estimate. The true elastic part of DD_CC constitutive law is ignored. The average hardening modulus is used as the pseudo-elastic modulus and the Poisson's ratio is set to 0.499 to describe plastic impressibility and avoid numerical issues (Figure 5(a)). To undertake this initialization step, the BCs shown in Figure 4(b) are reversed, and then applied to Ω_{def}^{exp} with the isotropic elastic law shown in Figure 5(a). Figure 5(b) indicates that the simple estimate of Ω_{ref}^0 does not deviate too much from the correct configuration and hence constitutes a fair (and cheap) initialization.

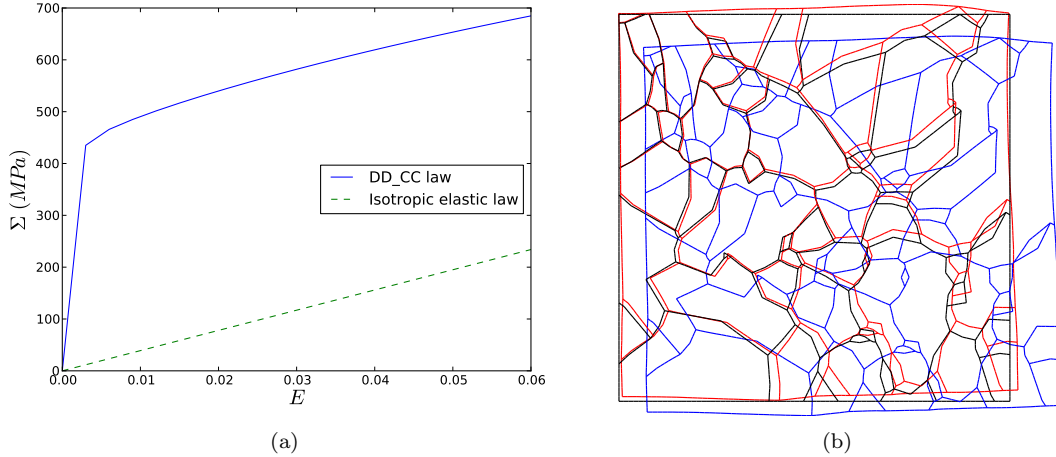(a)   (b)

Figure 5: Initialization of Ω_{ref}^0. (a) Stress-strain curve of DD_CC law and reference (tangent) pseudo-elastic law; (b) red: grain boundaries of Ω_{ref}^0. For comparison purposes, the black lines show Ω_{ref}^{exp}, the blue lines show Ω_{def}^{exp}, which can be measured by 3D-EBSD

3.4 Results

The results of this 2D synthetic case are shown in Figure 6. The procedure converges after only 3 iterations of the configuration estimation algorithm, as the difference between $\Omega_{def}^{(3)}$ and Ω_{def}^{exp} is less than the convergence criterion, as shown in Figure 6(b). However, the estimated initial configuration, $\Omega_{ref}^{(3)}$, is different from the exact solution, as shown in Figure 6(a). A slight yet visible difference also exists in the inverse pole figures, as shown in Figure 6(c) and Figure 6(d). In terms of the quality of the estimate for the reference configuration, a "distance" measurement is defined, which is the root mean square distance of corresponding vertices defining the microstructure between the exact configuration and the estimate in the reference configuration. To make this indicator dimensionless, it is normalized by the same distance computed for the known deformed configuration. Therefore, a normalized distance error of 100% is obtained when comparing the reference microstructure with the deformed microstructure obtained after a macroscopic strain of 6%. As a consequence, small changes between microstructures are emphasized with high error values resulting from the normalization choice. The initial estimate obtained by isotropic elastic compression reduces this relative coordinate error down to 55.7%, and the iterative determination lowers it further down to 42.9% of the coordinates error. Similarly, an orientation error is defined and normalized by the deformed state. At convergence, the orientation error also decreases as shown in Table I, but in a lesser degree. In other words, the error of reference configuration estimate drops and stabilizes during the iterations but does not vanish completely.
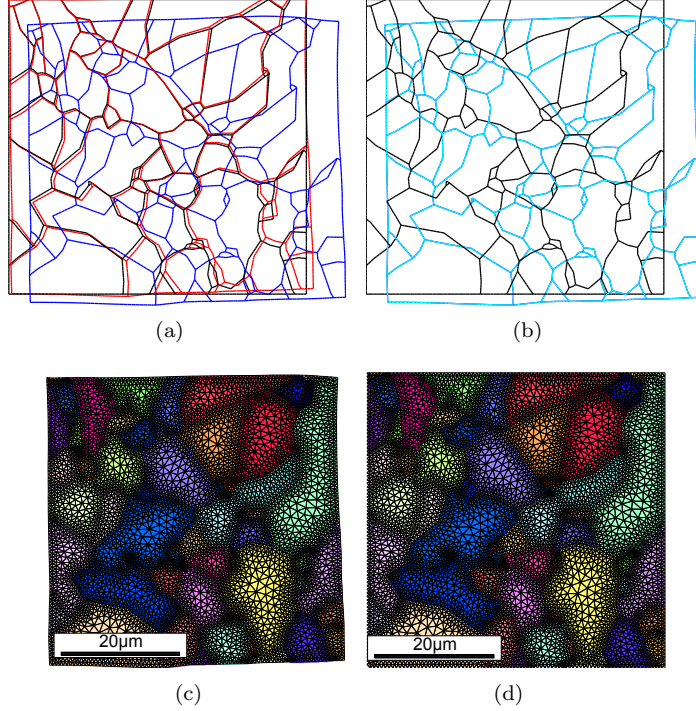
Figure 6: Backtracked reference configuration. (a) Grain boundaries of $\Omega_{ref}^{(3)}$ is shown in red lines. (b) Grain boundaries of $\Omega_{def}^{(3)}$ is shown in cyan lines. For comparison purposes, Ω_{ref}^{exp} is shown in black lines and Ω_{def}^{exp} is shown in blue lines in both figures. Note that $\Omega_{def}^{(3)}$ coincides with Ω_{def}^{exp} in (b). (c) $\Omega_{ref}^{(3)}$ is shown as an orientation map. (d) Ω_{ref}^{exp} is shown as an orientation map for comparison purposes

Table I: Distances of several configurations to Ω_{ref}^{exp}

Configuration	Ω_{def}^{exp}	Ω_{ref}^{0}	$\Omega_{ref}^{(1)}$	$\Omega_{ref}^{(2)}$	$\Omega_{ref}^{(3)}$
RMS distance to Ω_{ref}^{exp} (μm)	1.17	0.65	0.51	0.50	0.50
Normalized distance error	100%	55.7%	43.7%	42.9%	42.9%
RMS misorientation to Ω_{ref}^{exp} (°)	2.61	2.61	1.69	1.68	1.68
Normalized orientation error	100%	100%	64.8%	64.4%	64.4%

The estimated reference configuration at convergence, $\Omega_{ref}^{(3)}$ is shown in Figure 6. In terms of deviation from the correct reference configuration Ω_{ref}^{exp}, $\Omega_{ref}^{(3)}$ is 23 % lower than Ω_{ref}^{0} and 57% lower than Ω_{def}^{exp}. This error results from boundary conditions that cannot be determined exactly. The crystal plasticity analyses are sensitive to boundary conditions, which are unknown except at the measurement surface. The only differences between the two cases are the initial configuration and the BCs. Because the direct problem is treated without approximation, if the boundary conditions were exact so would be the computed initial microstructure. Hence the resulting discrepancy in the estimated and reference microstructure configuration does only result from differences in boundary conditions.

4   Conclusion

The present paper discussed the feasibility for the determination of undeformed microstructures from postmortem ones. A backtracking approach has been proposed to solve the inverse problem by iteratively updating the reference configuration via direct calculations. It is proposed to run FE analyses on the estimated reference configuration Ω_{ref}^{est} and get an estimated deformed configuration Ω_{def}^{est}, then modify Ω_{ref}^{est} based on the difference between Ω_{def}^{exp} and

Ω_{def}^{est}. Due to lack of in-depth information, displacements at surface are extruded to provide approximate boundary conditions for the FE simulations.

A virtual experiment on a 2D model serves as proof of concept. A sophisticated constitutive law, DD_CC, has been adopted to generate "experimental" data. Only the data at the top line (*i.e.,* the measurable surface) are considered to be known. Besides, the deformed model, including the in-depth microstructure, is considered known, as FIB-EBSD reveals the microstructure in experiments. It has been found that for relatively small plastic strains, simple constitutive laws such as isochoric elasticity restore much of the reference configuration. An iterative process of corrections based on DD_CC with correct parameters is then performed to improve the microstructure estimate. This process results in an estimated model that is closer to the exact one, with errors reduced by 57 %. More accurate boundary conditions need be adopted if the error is to be reduced further. As approximate boundary conditions are guessed an exact undeformed configuration cannot be obtained. Nonetheless, this algorithm is a step forward compared to the commonly used extruded microstructure from surface and the artificially generated Voronoi-style microstructure. From the better reconstructed model and with all information available at the surface, crystal plasticity can be studied more precisely. For example, identification based on the backtracked reference configuration results in more precise parameters, than those based on extruded model from surface, according to a companion paper [15].

It should be noted that this first part adopts correct constitutive equations for the determination of reference microstructures. In practice parameters of constitutive equations are often unknown and need to be identified by synergy between experiments and simulation. The identification of constitutive law parameters based on depth-resolved microstructures is discussed in a companion paper [15].

Acknowledgments

References

1. E. Héripré, M. Dexet, J. Crépin, L. Gélébart, A. Roos, M. Bornert, and D. Caldemaison. *Int. J. Plast.*, 23(9), 1512 (2007).

2. H. Lim, J.D. Carroll, C.C. Battaile, B.L. Boyce, and C.R. Weinberger. *Int. J. Mech. Sci.*, 92(0), 98 (2015).

3. A. Guery, F. Hild, F. Latourte, and S. Roux. *Mech. Mater.*, 100, 55 (2016).

4. A. Zeghadi, F. N'Guyen, S. Forest, A.-F. Gourgues, and O. Bouaziz. *Philos. Mag.*, 87(8), 1425 (2007).

5. R. A. Lebensohn, R. Brenner, O. Castelnau, and A. D. Rollett. *Acta Mater.*, 56(15), 3914 (2008).

6. M. A. Groeber, B. K. Haley, M. D. Uchic, D. M. Dimiduk, and S. Ghosh. *Mater. Charact.*, 57(4-5), 259 (2006).

7. M. Calcagnotto, D. Ponge, E. Demir, and D. Raabe. *Mater. Sci. Eng., A*, 527(10-11), 2738 (2010).

8. H. Altendorf, F. Latourte, D. Jeulin, M. Faessel, and L. Saintoyant. *Image Anal. Stereol.*, 33, 121 (2014).

9. A. Allais, M. Bornert, T. Bretheau, and D. Caldemaison. *Acta Metall. Mater.*, 42(11), 3865 (1994).

10. T. Hoc, J. Crépin, L. Gélébart, and A. Zaoui. *Acta Mater.*, 51(18), 5477 (2003).

11. Q. Shi, F. Latourte, F. Hild, and S. Roux. *Meas. Sci. Technol.*, 27(9), 095006 (2016).

12. W.Z. Abuzaid, M.D. Sangid, J.D. Carroll, H. Sehitoglu, and J. Lambros. *J. Mech. Phys. Solids*, 60(6), 1201 (2012).

13. J. Carter, M.W. Kuper, M.D. Uchic, and M.J. Mills. *Mater. Sci. Eng., A*, 605(0), 127 (2014).

14. A.J. Wilkinson, G. Meaden, and D.J. Dingley. *Ultramicroscopy*, 106(4-5), 307 (2006).

15. Q. Shi, F. Latourte, F. Hild, and S. Roux. LMT Cachan, France, unpublished research, 2017.

16. Code_Aster. www.code-aster.org. Accessed 1 June 2016.

17. F. Latourte, T. Salez, A. Guery, N. Rupin, and M. Mahé. *J. Nucl. Mater.*, 454(1-3), 373 (2014).

18. G. Monnet, L. Vincent, and B. Devincre. *Acta Mater.*, 61(16), 6178 (2013).